

Journal Pre-proof

Utilization of the common functional groups in bioactive molecules: Exploring dual inhibitory potential and computational analysis of keto esters against α -glucosidase and carbonic anhydrase-II enzymes

Imtiaz Khan, Ajmal Khan, Sobia Ahsan Halim, Majid Khan, Sumera Zaib, Balqees Essa Mohammad Al-Yahyaeei, Ahmed Al-Harrasi, Aliya Ibrar



PII: S0141-8130(20)35095-9

DOI: <https://doi.org/10.1016/j.ijbiomac.2020.11.170>

Reference: BIOMAC 17333

To appear in: *International Journal of Biological Macromolecules*

Received date: 23 October 2020

Revised date: 21 November 2020

Accepted date: 24 November 2020

Please cite this article as: I. Khan, A. Khan, S.A. Halim, et al., Utilization of the common functional groups in bioactive molecules: Exploring dual inhibitory potential and computational analysis of keto esters against α -glucosidase and carbonic anhydrase-II enzymes, *International Journal of Biological Macromolecules* (2018), <https://doi.org/10.1016/j.ijbiomac.2020.11.170>

This is a PDF file of an article that has undergone enhancements after acceptance, such as the addition of a cover page and metadata, and formatting for readability, but it is not yet the definitive version of record. This version will undergo additional copyediting, typesetting and review before it is published in its final form, but we are providing this version to give early visibility of the article. Please note that, during the production process, errors may be discovered which could affect the content, and all legal disclaimers that apply to the journal pertain.

Utilization of the common functional groups in bioactive molecules: Exploring dual inhibitory potential and computational analysis of keto esters against α -glucosidase and carbonic anhydrase-II enzymes

Imtiaz Khan,^{a,*} Ajmal Khan,^b Sobia Ahsan Halim,^b Majid Khan,^{b,c} Sumera Zaib,^d
Balqees Essa Mohammad Al-Yahyaee,^b Ahmed Al-Harrasi,^{b,*} Aliya Ibrar,^{e,*}

^a*Department of Chemistry and Manchester Institute of Biotechnology, The University of Manchester, 131 Princess Street, Manchester M1 7DN, United Kingdom*

^b*Natural and Medical Sciences Research Center, University of Nizwa, P.O Box 33, Postal Code 616, Birkat Al Mauz, Nizwa, Oman*

^c*H. E. J. Research Institute of Chemistry, International Center for Chemical and Biological Sciences, University of Karachi, Karachi-75270, Pakistan*

^d*Department of Biochemistry, Faculty of Life Sciences, University of Central Punjab, Lahore-54590, Pakistan*

^e*Department of Chemistry, Faculty of Natural Sciences The University of Haripur, Haripur, KPK-22620, Pakistan*

***Correspondence:** *imtiaz.khan@manchester.ac.uk* (I. Khan); *aharrasi@unizwa.edu.om* (A. Al-Harrasi); *jadoonquaidian@gmail.com* (A. Ibrar).

Abstract

Diabetes mellitus, a progressive chronic disease, characterized by the abnormal carbohydrate metabolism is associated with severe health complications including long term dysfunction or failure of several organs, cardiovascular and micro-angiopathic problems (neuropathy, nephropathy, retinopathy). Despite the existence of diverse chemical structural libraries of α -glucosidase inhibitors, the limited diabetic treatment due to the adverse side effects such as abdominal distention, flatulence, diarrhoea, and liver damage associated with these inhibitors encourage the medicinal research community to design and develop new and potent inhibitors of α -glucosidase with better pharmacokinetic properties. In this perspective, we demonstrate the successful integration of common functional groups (ketone & ester) in one combined pharmacophore which is favourable for the formation of hydrogen bonds and other weaker interactions with the target proteins. These keto ester derivatives were screened for their α -glucosidase inhibition potential and the *in vitro* results revealed compound **3c** as the highly active inhibitor with an IC_{50} value of $12.4 \pm 0.16 \mu\text{M}$ compared to acarbose ($IC_{50} = 942 \pm 0.74 \mu\text{M}$). This inhibition potency was ~76-fold higher than acarbose. Other potent compounds were **3f** ($IC_{50} = 28.0 \pm 0.28 \mu\text{M}$), **3h** ($IC_{50} = 33.9 \pm 0.09 \mu\text{M}$), **3g** ($IC_{50} = 34.1 \pm 0.04 \mu\text{M}$), and **3d** ($IC_{50} = 76.5 \pm 2.0 \mu\text{M}$). In addition, the emerging use of carbonic anhydrase inhibitors for the treatment of diabetic retinopathy (a leading cause of vision loss) prompted us to screen the keto ester derivatives for the inhibition of carbonic anhydrase-II. Compound **3b** was found significantly active against carbonic anhydrase-II with an IC_{50} of $16.5 \pm 0.92 \mu\text{M}$ (acetazolamide; $IC_{50} = 18.2 \pm 1.23 \mu\text{M}$). Compound **3a** also exhibited comparable potency with an IC_{50} value of $18.9 \pm 1.08 \mu\text{M}$. Several structure-activity relationship analyses depicted the influence of the substitution pattern on both the aromatic rings. Molecular docking analysis revealed the formation of several H-bonding interactions through the ester carbonyl and the nitro oxygens of **3c** with the side chains of His348, Arg212 and His279 in the active pocket of α -glucosidase whereas **3b** interacted with His95, -OH of Thr197, Thr198 and WAT462 in the active site of carbonic anhydrase-II. Furthermore, evaluation of ADME properties suggests the safer pharmacological profile of the tested derivatives.

Keywords: Diabetes mellitus; α -Glucosidase; Carbonic anhydrase; Keto esters; Diabetic retinopathy; PAINS; ADME properties; Structure-activity relationships.

1. Introduction

Diabetes mellitus (DM), a multifactorial chronic metabolic disorder, largely characterized by the abnormal carbohydrate metabolism remained as one of the rapidly growing serious global health threats [1]. According to International Diabetes Federation (IDF) and World Health Organization

(WHO), the expected number of diabetic patients could be up to 693 million in 2045 and this steady increase contributes enormously towards the overall risk of dying prematurely [2]. Type II diabetes mellitus contributes about 80-90% of all diabetic cases where body cannot use the insulin properly resulting in the poor control over glucose metabolism [3-5], thus rendering the diabetic patients more vulnerable to severe health complications such as increased risk of common infections, cancer, kidney failure, leg amputation, vision loss, and the development of micro-angiopathic problems such as neuropathy, nephropathy and retinopathy [6-10]. Current anti-diabetic drugs available for the treatment of type 2 diabetes include insulin secretagogues (sulfonylureas, biguanides, thiazolidinediones) and insulin mimetics (glucagon-like peptide analogues and agonists, α -glucosidase, sodium-glucose cotransporter, and DPP IV inhibitors) [11]. Despite intensive lifestyle modifications combined with oral medication, there remained a challenge in the scientific community to develop more potent and less toxic clinical agents with reduced side effects to treat diabetic complications more effectively.

As such the inhibition of α -glucosidase (EC 3.2.1.20), an intestinal cell membrane enzyme responsible for the hydrolysis of polysaccharides into monosaccharides, is considered as an essential target for the discovery of novel inhibitors for the treatment of non-insulin-dependent diabetes mellitus (type II) [12,13]. These inhibitors slow down the digestion of carbohydrates which in turn suppress the postprandial hyperglycemia thereby reducing the absorption of gut glucose into the blood [14,15]. Several α -glucosidase inhibitors including metformin, acarbose, voglibose, and miglitol are commercially available for the treatment of type 2 diabetes (Fig. 1). However, the serious side effects such as abdominal distention, flatulence and diarrhoea have inspired the medicinal research community to design and develop several synthetic heterocyclic and non-heterocyclic inhibitors with better pharmacological profile [16-22].

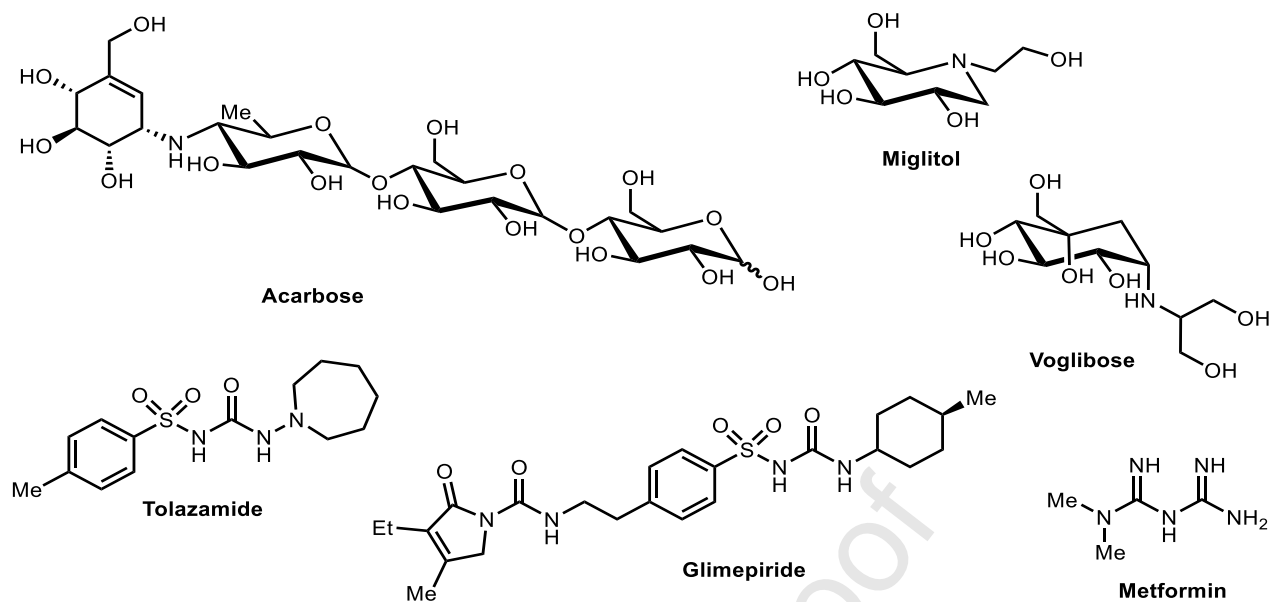


Fig. 1. Examples of clinical drugs for type 2 diabetes mellitus.

Diabetic retinopathy (DR), characterized by retinal ischemia, proliferation of retinal vessels and increased retinal vascular permeability, is the leading cause of vision loss among working-age populations in developed countries [23,24]. Despite having limited treatment options such as tight glycaemic, blood pressure control and destructive laser surgery, this disease is prevalent in almost all patients with type 1 diabetes and over 60% with type 2 diabetes [25,26]. Among the emerging effective treatment options, the inhibition of carbonic anhydrases (EC 4.2.1.1), zinc-containing metalloenzymes, is considered as promising therapeutic approach by lowering the intraocular pressure [27]. These ubiquitous enzymes are actively involved in the rapid conversion of carbon dioxide to bicarbonate and protons, thus playing an important role in several physiological and pathological processes [28,29]. Out of 16 isozymes, CA I, II, IV and XIV have been identified in the human eye [30] and are responsible for bicarbonate secretion regulating aqueous humor production and intraocular pressure. Well-recognized CA II inhibitors including acetazolamide, methazolamide and dichlorphenamide showed promising effects in treating glaucoma, characterized by excessive aqueous humor and elevated intraocular pressure (IOP) through multiple mechanisms [23,31] (Fig. 2). Therefore, design and development of new small molecule inhibitors offer therapeutic promise for the treatment of diabetic retinopathy.

Inspired by the above-mentioned literature precedents and in continuation of our efforts on the development of α -glucosidase inhibitors [32,33], in the present study we investigated a series of keto esters which are versatile intermediates in organic chemistry, agrochemicals, and pharmaceuticals [34-44]. To the best of our knowledge, this motif has not been evaluated for the identification of α -

glucosidase and carbonic anhydrase inhibitors. Therefore, the utilization of the common functional groups (keto esters) in bioactive molecules was explored while investigating their scope as potential inhibitors of α -glucosidase and carbonic anhydrase for the treatment of diabetes mellitus and diabetic retinopathy, respectively. *In vitro* biological activity results were rationalized using molecular docking approach where the binding interactions of the potent inhibitors with the specific amino acid residues were the key stabilizing factor in the active pocket of the enzyme. Furthermore, evaluation of ADME properties of all the screened derivatives suggests their safer pharmacological profile.

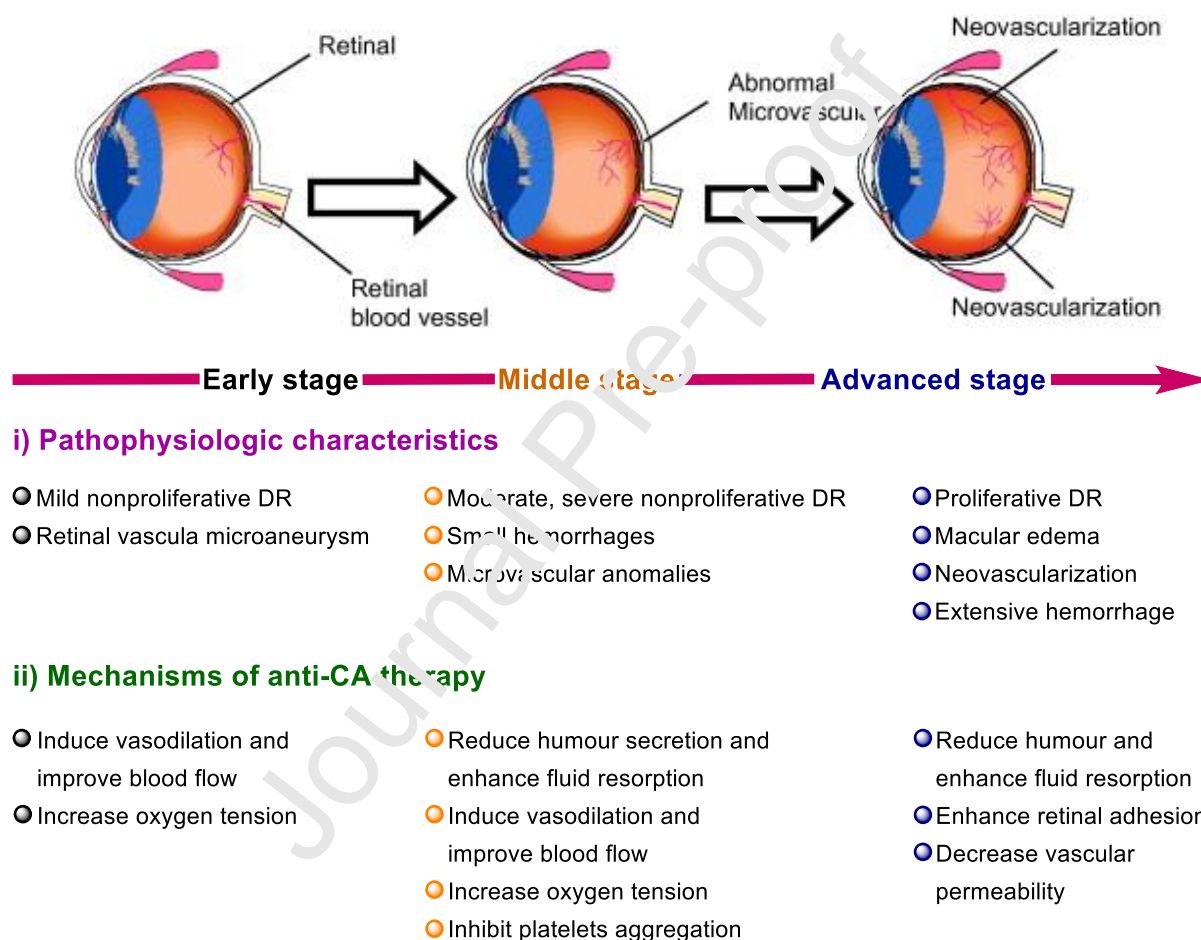


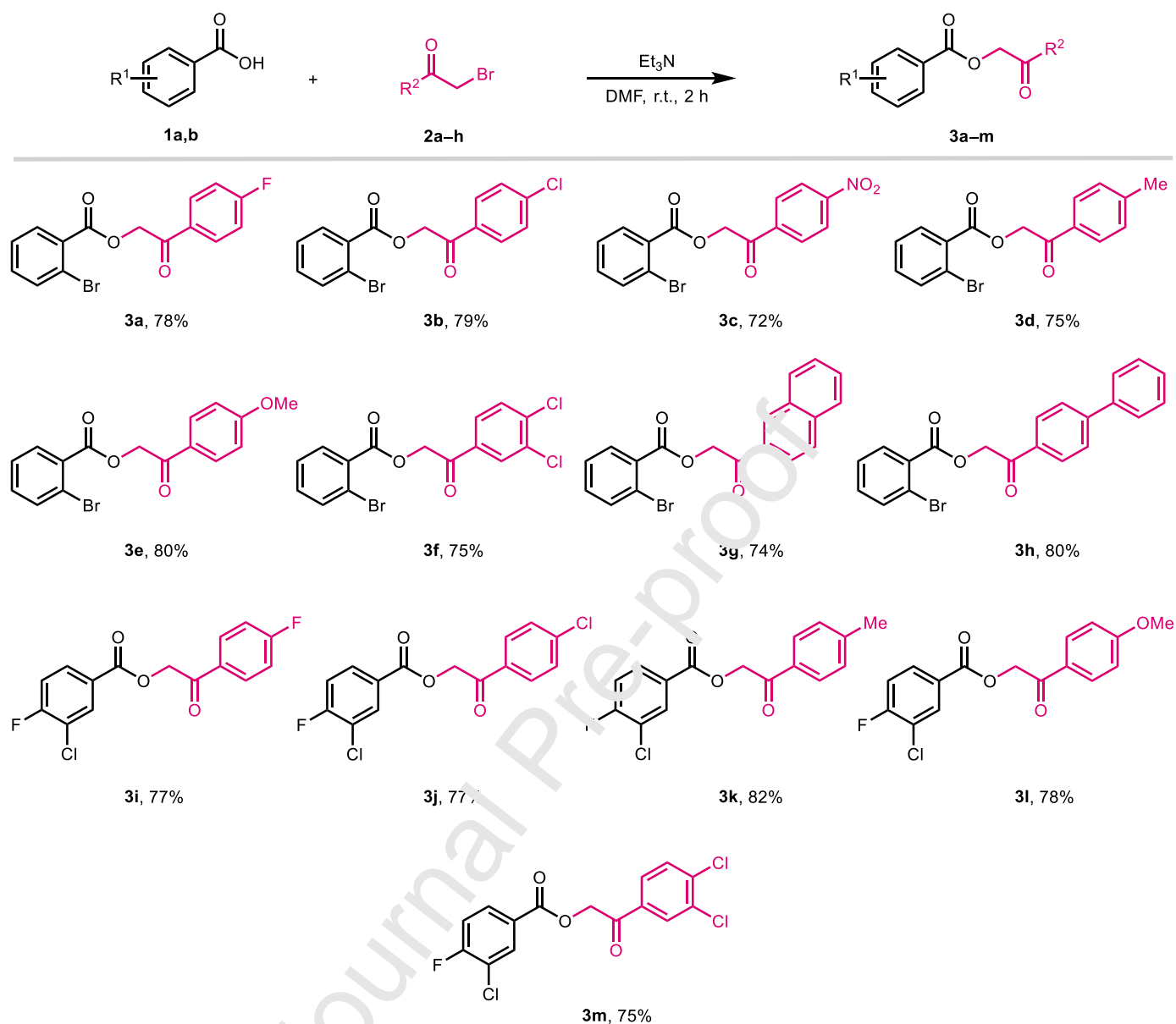
Fig. 2. Schematic illustration of pathophysiologic characteristics of diabetic retinopathy and mechanisms of anti-CA therapy in each stage (color pattern depicts the events at different stages). Reproduced with permission from Ref. [23]. Copyright 2009, Elsevier Ltd.

2. Results and discussion

2.1. Synthetic chemistry

The synthetic route for the synthesis of keto esters **3a–m** is depicted in Scheme 1. Halogenated acids **1a,b** were successfully coupled with diversely substituted phenacyl bromides **2a–h** in the presence of triethylamine in DMF at room temperature [45-47]. The phenacyl bromides used were either purchased

from commercial source or prepared *via* the bromination of acetophenones [48]. The desired keto esters **3a–m** were furnished in good yields. The structural diversity was inherited from acetophenones which possess a range of electron-donating and electron-withdrawing groups on the aromatic ring. The condensation of aromatic acids with phenacyl bromides was evidenced by the evaluation of FTIR spectra where characteristic stretching bands for two carbonyls ($\nu\text{C}=\text{O}_{\text{Keto}}$ and $\nu\text{C}=\text{O}_{\text{Ester}}$) were observed in the range of $1702\text{--}1682\text{ cm}^{-1}$ and $1732\text{--}1717\text{ cm}^{-1}$, respectively. Additionally, the spectra were devoid of stretching absorption for COOH in the range of $3400\text{--}2400\text{ cm}^{-1}$. ^1H NMR analysis also revealed the successful coupling of aromatic acids with phenacyl bromides where methylene signals were observed in the range of $5.75\text{--}5.53\text{ ppm}$ as singlet alongside the disappearance of characteristic COOH proton. Further evidence was acquired from ^{13}C NMR data where the two distinctive signals for keto and ester carbonyl carbons appeared in the range of $195.3\text{--}182.9\text{ ppm}$ and $167.9\text{--}163.3\text{ ppm}$, respectively. The methylene carbon also resonated in the range of $66.8\text{--}66.4\text{ ppm}$. Moreover, the mass spectroscopic data also confirmed the formation of keto ester products.



Scheme 1. Synthesis and scope of keto esters **3a-m**.

2.2. Enzymatic activity

The use of small molecule inhibitors with dual mode of action in drug discovery programs remained a driving force for the identification of new classes of compounds incorporating medically relevant pharmacophores. The presence of various functional groups (FGs) as bioactive pharmacophores contribute enormously to the physicochemical properties and intrinsic reactivity of the parent molecule. These functional groups have actively been involved in the formation of different interactions with target proteins. Thus, the combination of more than one functional group in a specific molecule offers a pressing opportunity to increase the drug discovery space by introducing new combinatorial libraries of

compounds. These indispensable literature findings on the use of various functional groups in medicinal chemistry and drug discovery arena prompted us to generate new structures **3a–m** incorporating ketone and ester functionalities and assess their α -glucosidase and carbonic anhydrase-II inhibitory potential. The *in-vitro* screening results are presented in Table 1. Acarbose and acetazolamide were used as standard inhibitors with IC_{50} values of 942 ± 0.74 and $18.2 \pm 1.23 \mu\text{M}$, against α -glucosidase and carbonic anhydrase-II, respectively. The results demonstrated a striking variation in the inhibitory activities with IC_{50} values ranging from 12.4–381.7 and 16.5–103.8 μM , against α -glucosidase and carbonic anhydrase-II enzymes, respectively. In case of α -glucosidase, all active compounds (**3b–i**) showed much higher activity than the standard acarbose while compound **3b** was found significantly active against carbonic anhydrase-II with IC_{50} of $16.5 \pm 0.92 \mu\text{M}$. The predictive structure-activity relationship (SAR) of the tested compounds was investigated considering the attached functional groups at different positions of both aryl rings as the key contributing functionalities towards the inhibition of the corresponding enzyme.

2.3. Structure-activity relationship analyses and molecular docking studies

The role of various substituents on the aromatic rings connected with both ketone and ester functionalities on the inhibition of α -glucosidase and carbonic anhydrase-II enzymes was investigated and several structure-activity relationship analyses were observed. *In vitro* activity data presented in Table 1 for the inhibition of α -glucosidase enzyme revealed compound **3c** as the highly active inhibitor with an IC_{50} value of $12.4 \pm 0.16 \mu\text{M}$ followed by **3f** ($IC_{50} = 28.0 \pm 0.28 \mu\text{M}$), **3h** ($IC_{50} = 33.9 \pm 0.09 \mu\text{M}$), **3g** ($IC_{50} = 34.1 \pm 0.04 \mu\text{M}$), and **3d** ($IC_{50} = 76.5 \pm 2.0 \mu\text{M}$). The most potent compound **3c** incorporates a bromo substituent at the *ortho*-position of the phenyl ring derived from carboxylic acid component whereas a highly polarizable electron-deficient nitro group was present at the *para*-position of the aromatic ring (R^2). Keeping the acid derived component unchanged, the nitro group was replaced with hydrophobic electron-donating aromatic (phenyl) and aliphatic (methyl) groups and a descending trend in the inhibitory potential was observed (**3c**>**3h**>**3d**) (Fig. 3).

Table 1. α -Glucosidase and carbonic anhydrase-II inhibitory potential of keto esters **3a–m**.

 3a-m				
Compound	Substituents		α -Glucosidase inhibition	Carbonic anhydrase-II inhibition
	R ¹	R ²	IC ₅₀ ± SEM (μM)	
3a	2-Br	4-F-Ph	NA	18.9 ± 1.08
3b	2-Br	4-Cl-Ph	381.7 ± 8.1	16.5 ± 0.92
3c	2-Br	4-NO ₂ -Ph	12.4 ± 0.16	44.0 ± 1.12
3d	2-Br	4-Me-Ph	76.5 ± 2.0	37.0 ± 2.48
3e	2-Br	4-OMe-Ph	112.4 ± 9.5	103.8 ± 2.88
3f	2-Br	3,4-diCl-Ph	28.0 ± 0.28	60.0 ± 0.72
3g	2-Br	Naphthyl	34.1 ± 0.04	NA
3h	2-Br	Biphenyl	33.9 ± 0.09	NA
3i	3-Cl,4-F	4-F-Ph	168.8 ± 4.0	NA
3j	3-Cl,4-F	4-Cl-Ph	NA	53.3 ± 0.86
3k	3-Cl,4-F	4-Me-Ph	NA	90.9 ± 2.83
3l	3-Cl,4-F	4-OMe-Ph	NA	40.4 ± 0.28
3m	3-Cl,4-F	3,4-diCl-Ph	NA	58.8 ± 1.95
Acarbose	—		942 ± 0.74	—
Acetazolamide	—		—	18.2 ± 1.23

NA = Not active.

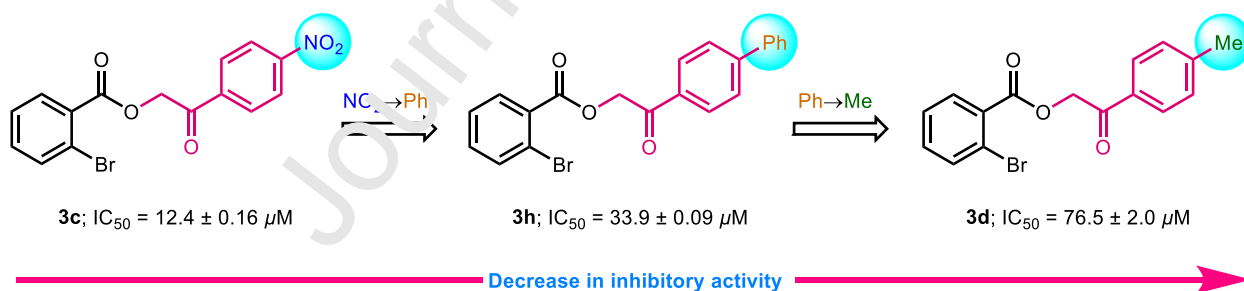


Fig. 3. Decreasing effect of substitution pattern on the α -glucosidase inhibition.

Similarly, swapping the nitro group with an electron-rich methoxy (**3e**; IC₅₀ = 112.4 ± 9.6 μM) as well as introduction of a di-substitution in the form of chloro group at *meta*- and *para*-position (**3f**; IC₅₀ = 28.0 ± 0.28 μM) also produced reduced inhibition of α -glucosidase compared to **3c** (IC₅₀ = 12.4 ± 0.16 μM), however, all the compounds were significantly more active than standard drug (acarbose). Compound **3g** bearing a bulky naphthyl group instead of a 4-nitrophenyl ring also furnished the excellent inhibitory results comparable to **3h** while ~28-folds higher potency compared to acarbose

(Fig. 4). Moreover, second set of compounds derived from di-halogenated acid were less productive and only compound **3i** showed activity against α -glucosidase enzyme with an IC_{50} value of $168.8 \pm 4.0 \mu\text{M}$ (Fig. 4). Compound **3b** was identified as the least active inhibitor with an IC_{50} value of $381.7 \pm 8.1 \mu\text{M}$.

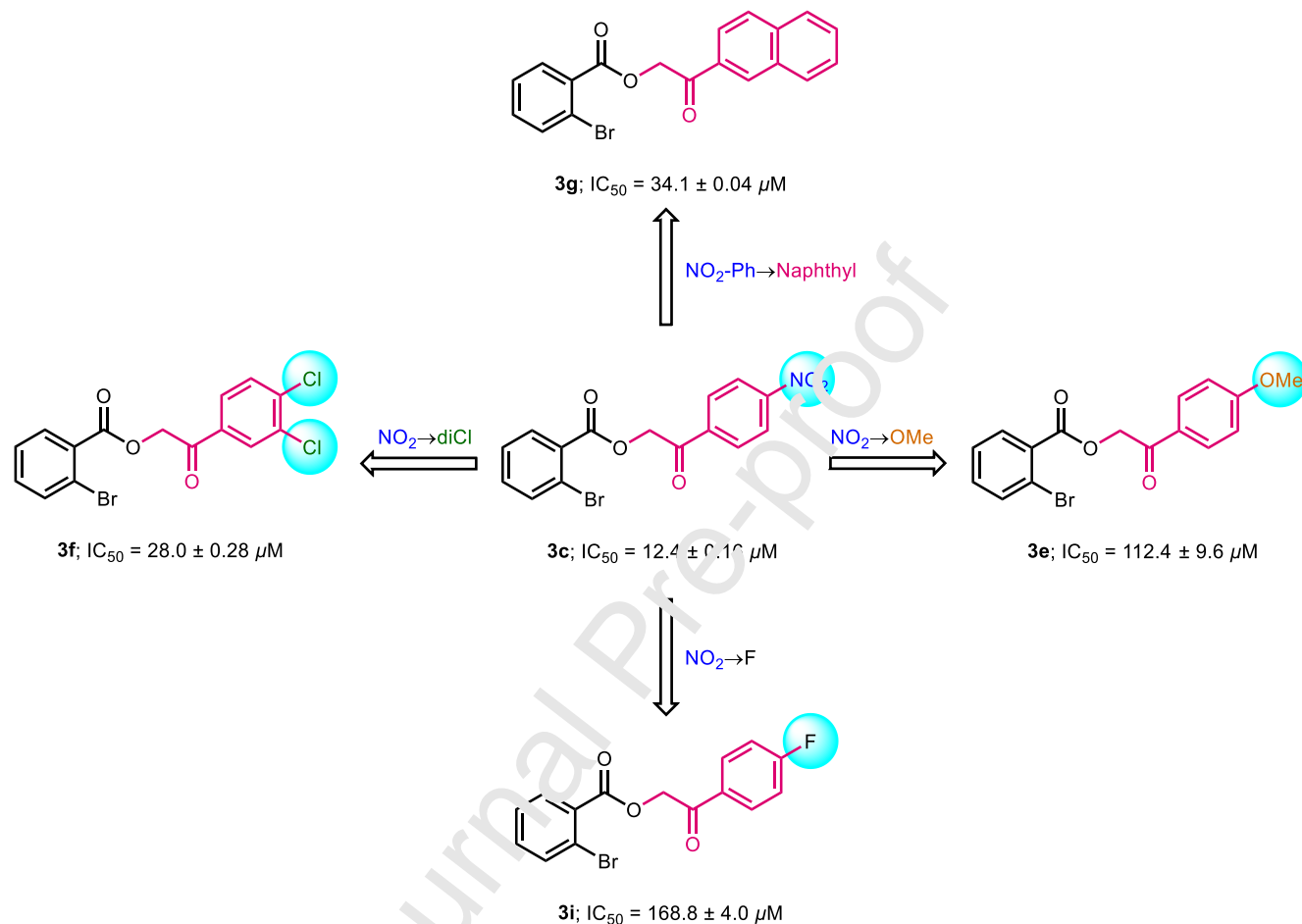


Fig. 4. Decreasing effect of substitution pattern on the α -glucosidase inhibition.

To understand the observed *in vitro* inhibitory activity results, role of various substitution patterns and binding interactions in the active site of α -glucosidase, molecular docking analysis was performed. For this purpose, we used the homology model of *S. cerevisiae* α -glucosidase due to the unavailability of the crystal structure. The most potent compound **3c** was found to be well accommodated in the active site of α -glucosidase. The binding mode of **3c** showed that the ester carbonyl and the nitro oxygens mediated multiple H-bonding with the side chains of His348, Arg212 and His279. Additionally, it was also observed that the keto esters derived from 3-chloro-4-fluorobenzoic acid did not show favorable binding interactions and both substituents cause steric hindrance in the active site of α -glucosidase enzyme, thus rendering these derivatives surface exposed.

Similarly, the side chains of Arg212 and His348 provided H-bonds to the oxygen of ester carbonyl in compound **3f**. Likewise, the ester moieties of **3h** and **3g** were found to be H-bonded with the side chain of Arg212. Additionally, a water molecule and Phe157 also offered H-bond and hydrophobic interaction to compound **3h** whereas the ester carbonyls of **3d** and **3e** were stabilized by the side chain of His348 through H-bonding. Similarly, the side chains of Arg212 and His348 offered H-bonds to the ester moiety of the least active inhibitors **3i** and **3b**. The docked view of the most active hit is shown in Fig. 5.

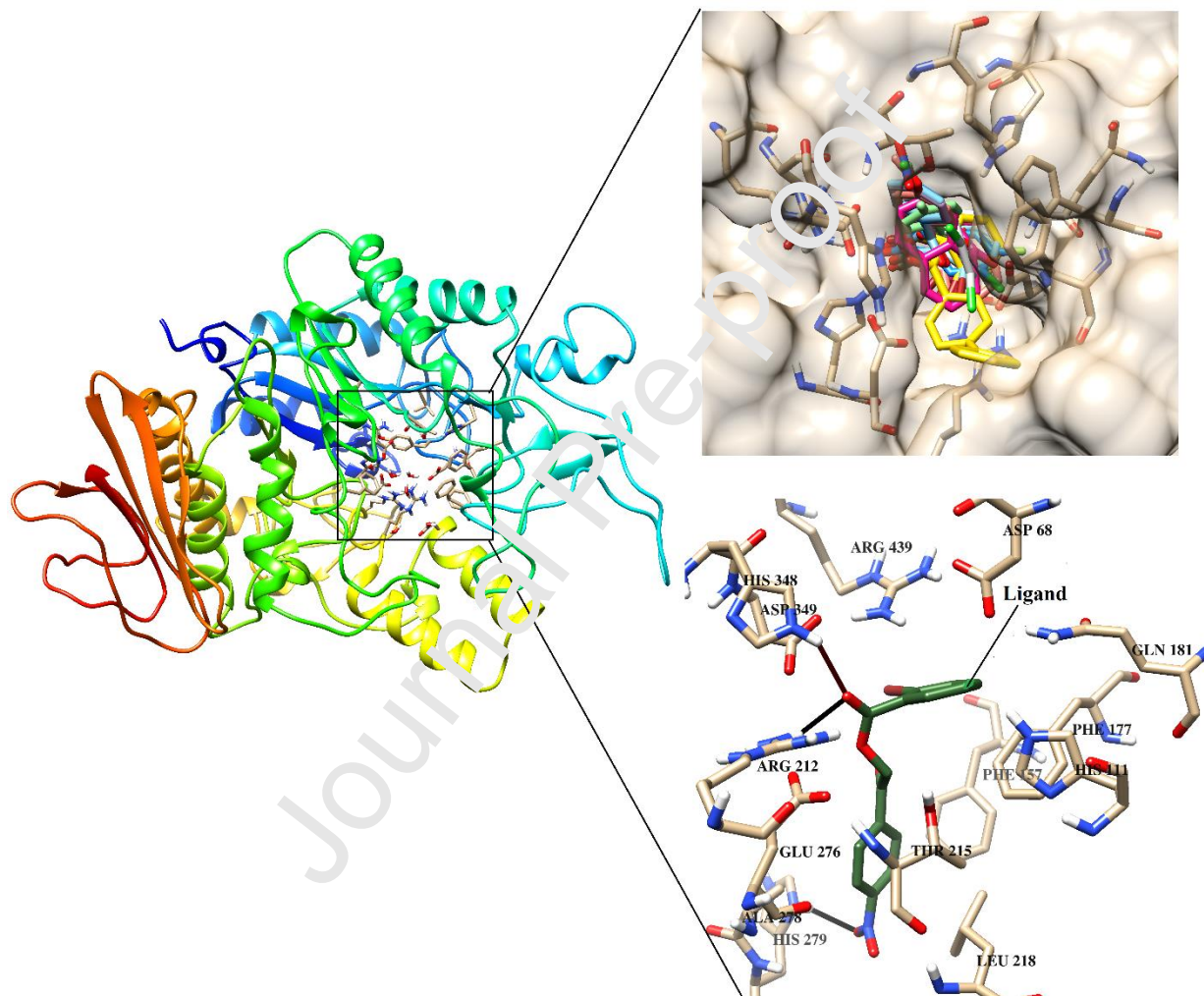


Fig. 5. The active site residues of α -glucosidase enzyme are shown in the box. The binding modes of compounds **3b–i** are depicted in the upper right panel, while the docked view of the most active hit **3e** is shown in the lower right panel. The hydrogen bonds are presented in black lines.

The synthesized compounds were also tested against carbonic anhydrase-II and the *in vitro* results revealed that several compounds (**3a–d**, **3f–j**, **3l**, **3m**) possess significant inhibitory affinities when compared to the standard drug (acetazolamide). Among the screened compounds, **3a** and **3b** exhibited highest potency with IC_{50} values of $18.9 \pm 1.08 \mu\text{M}$ and $16.5 \pm 0.92 \mu\text{M}$, respectively. Both derivatives

incorporate halogens (F & Cl) at the *para*-position of the aryl ring and in combination with the *ortho*-bromophenyl ring impart significant influence on the biological inhibition of CA-II enzyme. The loss of potency was observed when inductively withdrawing chloro substituent was replaced with moderately electron-donating (methyl) and highly polarizable electron-withdrawing (nitro) groups. These derivatives (**3d** & **3c**) demonstrated IC_{50} values of $37.0 \pm 2.48 \mu\text{M}$ and $44.0 \pm 1.12 \mu\text{M}$, respectively (Fig. 6). However, presence of a strongly electron-rich (methoxy) substituent imparted deleterious effect on the inhibition of CA-II enzyme (**3e**; $IC_{50} = 103.8 \pm 2.88 \mu\text{M}$). The inhibitory activity was regained when a bromophenyl ring in **3e** was replaced with a di-halogenated (3-Cl,4-F) phenyl ring (Fig. 7).

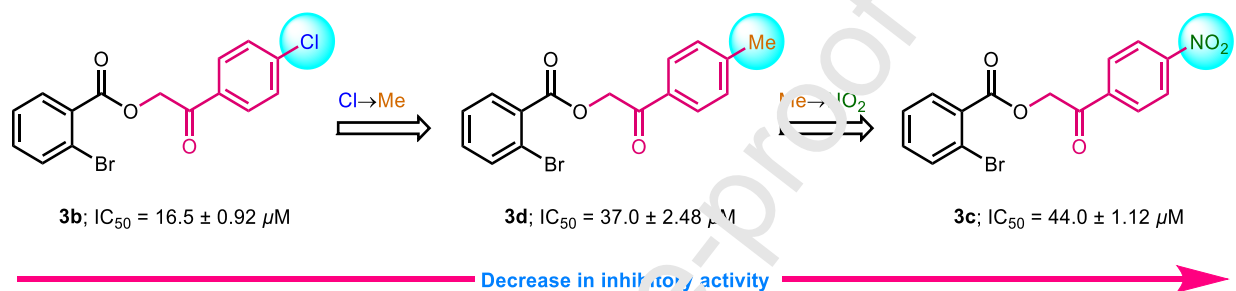


Fig. 6. Decreasing effect of substitution pattern on carbonic anhydrase-II inhibition.

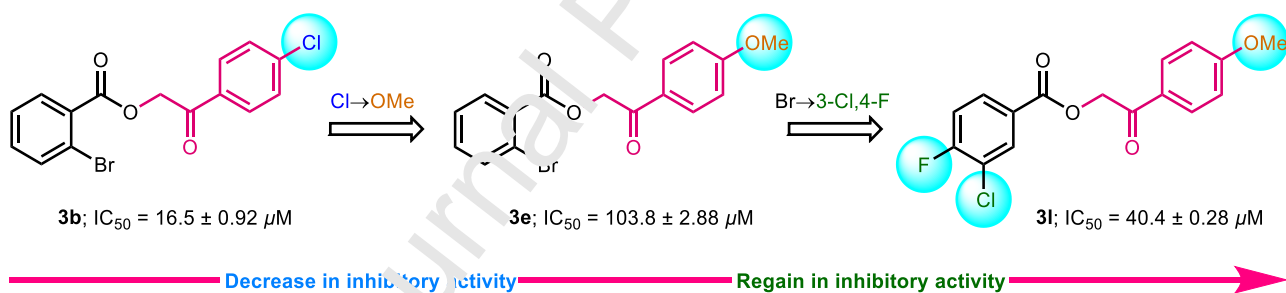


Fig. 7. Effect of substitution pattern on carbonic anhydrase-II inhibition.

Furthermore, the introduction of an additional chloro group at the *meta*-position of the phenyl ring already equipped with the same substituent at the *para*-position also proved detrimental, resulting in moderate inhibitory efficacy (**3f**; $IC_{50} = 60.0 \pm 0.72 \mu\text{M}$). The use of sterically demanding biphenyl and naphthyl groups as R^2 (**3g** & **3h**) remained completely impotent. In contrast, the keto ester derivatives (**3j–m**) derived from the di-halogenated acids were identified as the selective inhibitors of CA-II enzyme and showed no activity against α -glucosidase enzyme. In this set of compounds, electron-rich (methoxy) and halogen substituted derivatives (**3j**, **3l**, **3m**) produced moderate inhibitory efficacy demonstrating IC_{50} values in the range of $40.4\text{--}58.8 \mu\text{M}$ (Fig. 8). Compounds **3k** ($IC_{50} = 90.9 \pm 2.83 \mu\text{M}$) and **3e** ($IC_{50} = 103.8 \pm 2.88 \mu\text{M}$) were observed as the least active inhibitors of CA-II.

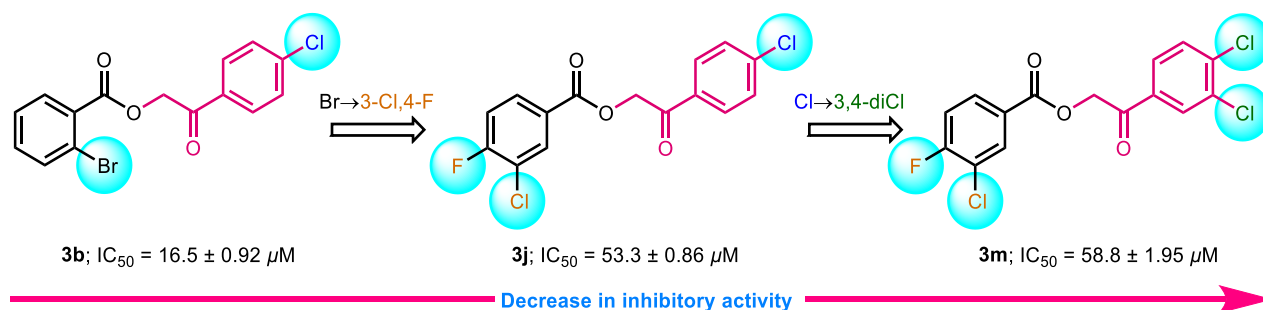


Fig. 8. Decreasing effect of substitution pattern on carbonic anhydrase-II inhibition.

For better understand of the binding of the potent inhibitors into the target enzyme (CA-II) and to rationalize the observed *in vitro* inhibitory activity results and influence of the different substituents, molecular docking studies were performed. For this purpose, we used the X-ray crystallographic structure of CA-II (PDB: 1V9E). The binding mode of **3b** revealed the formation of excellent binding interactions within the active site where the ester carbonyl moiety of **3b** mediated multiple H-bonding with the side chains of His95, -OH of Thr197 and a conserved water molecule, and a metal-ligand interaction with the Zn^{2+} ion in the active site of enzyme. The carbonyl oxygen of the compound was also found to be H-bonded with the side chain of Thr198 and WAT462. The docked view of **3b** is shown in Fig. 9. Similarly, the ester carbonyl of compound **3a** was bound with Zn^{2+} ion through metallic interactions while the side chains of His95 and Gln91 provided H-bond to the oxygen atom of the ester carbonyl. Additionally, His63 offered hydrophobic interaction to the compound. The binding modes of **3a** and **3b** were found to be nearly similar. On the other hand, compounds **3g-i** were not active in the carbonic anhydrase-II assay. The naphthyl, biphenyl and 4-fluorophenyl moieties as R^2 did not fit into the active site of CA-II. Moreover, the presence of 3-chloro and 4-fluoro substituents in **3i** also causes clashes with the active site residues.

The binding mode of **3d** and **3l** showed that the ester carbonyl mediated H-bonding with the side chain of Asn66 and the amino nitrogen of Thr197, respectively. The carbonyl oxygen of **3c** and the ester oxygen of **3j** interacted with the side chain of Gln91 through H-bonding while the side chain of His93 provided π - π interactions to these compounds. The ester oxygen of **3m** mediated multiple H-bonds with the side chains of His63 and Asn66 and hydrophobic interaction with the side chain of Phe129. Similarly, the side chain of Asn66 donated H-bond to the ester oxygen of **3f**. However, the side chains of Gln91 and His93 stabilized the carbonyl moiety of **3k** via H-bonding and hydrophobic interaction, respectively. Compound **3e** was the least active inhibitor of CA-II. The side chains of His63 and His93 established H-bonding and hydrophobic interaction, respectively, with the compound **3e**. It was observed that the substitution of more bulky groups as R^2 substituent is not favorable for the binding of

the compound and produced steric hinderance in the active site of CA-II, thus decrease the biological activities of the compounds. The docking scores and docking interactions of compounds are well correlated with the inhibitory affinities of the compounds. The binding interactions of **3a–m** in the active sites of α -glucosidase and CA-II are tabulated in Table S1.

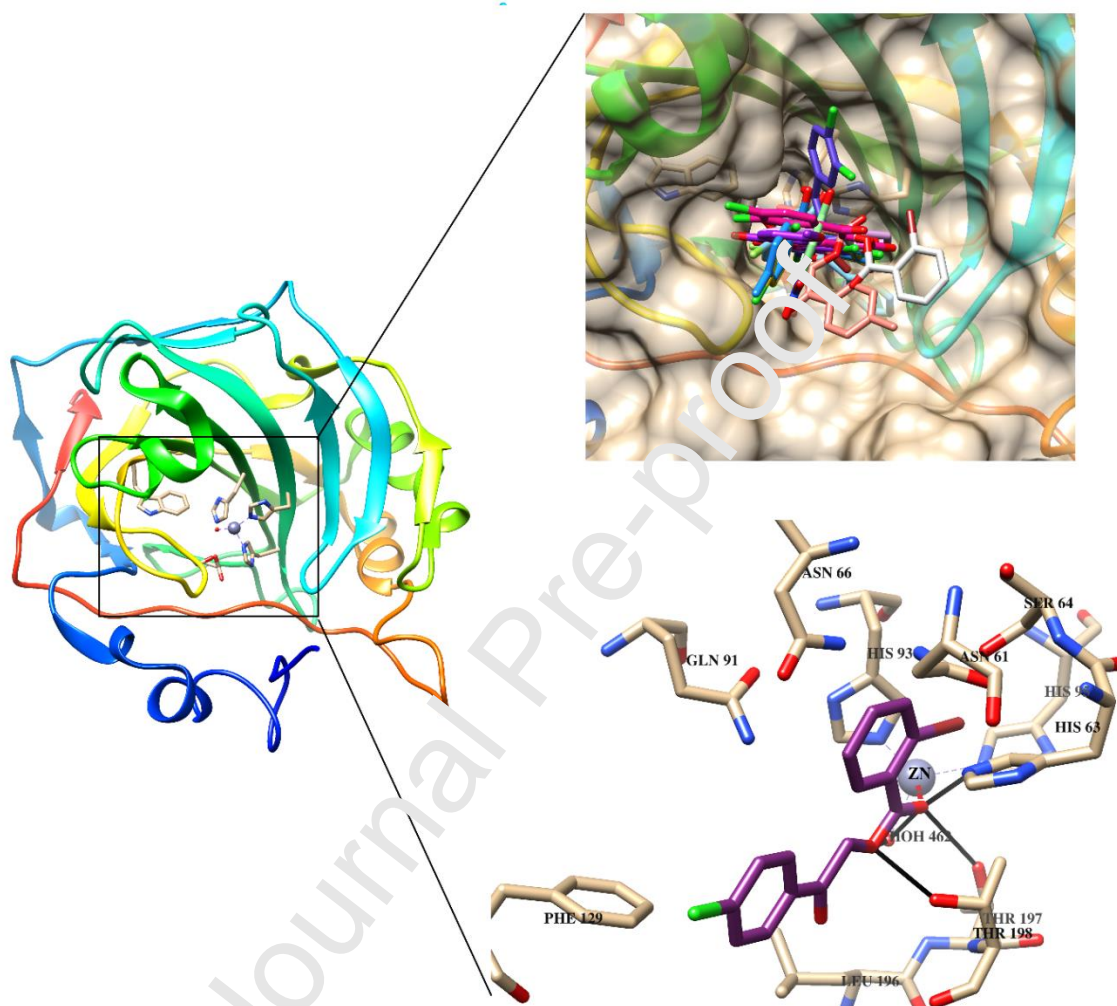


Fig. 9. The active site residues of carbonic anhydrase-II are shown in the box. The binding modes of compounds **3a–f** and **3j–m** are depicted in the upper right panel, while the docked view of the most active hit **3b** is shown in the lower right panel. The hydrogen bonds are presented in black lines while metal-ligand coordination is demonstrated in red dotted lines.

2.4. Kinetics studies

To investigate the type of inhibition and dissociation constant of the tested compounds, kinetics studies of the most active compounds **3b** (against *b*CA-II) and **3c** (against α -glucosidase) were performed at different concentrations of compounds and substrates. Kinetics study of compound **3b** against *b*CA-II showed that compound **3b** inhibited the *b*CA-II enzyme in a concentration-dependent manner with K_i value of $17.05 \pm 0.021 \mu\text{M}$. From the kinetics studies, it was also inferred that the compound **3b** is a

competitive inhibitor for *bCA-II*. The type of inhibition was determined by Lineweaver-Burk plots, the reciprocal of the rate of reaction was plotted against the reciprocal of substrate concentrations to monitor the effect of inhibitor on both K_m and V_{max} . The Lineweaver-Burk plots of **3b** against *bCA-II* clearly showed that the mode of inhibition of **3b** is competitive (Fig. 10A). In competitive inhibition, the K_m of enzyme increases without affecting V_{max} . The Lineweaver-Burk plots also showed that in the presence of compound **3b**, the K_m of *bCA-II* was increased significantly, while the V_{max} remains constant indicating the competitive inhibition.

On the other hand, Kinetics study of compound **3c** against α -glucosidase enzyme showed that compound **3c** is a mixed-type inhibitor with K_i value of $18.01 \pm 0.018 \mu\text{M}$. In a mixed-type inhibition, both the K_m and V_{max} are changed. The high K_m and low V_{max} of α -glucosidase in the presence of compound **3c** indicated a mixed-type of inhibition (Fig. 11A).

The K_i values were determined by secondary replots of Lineweaver-Burk plots by plotting the slope of each line in the Lineweaver-Burk plots against different concentrations of compounds **3b** and **3c** (Figs. 10B and 11B). The K_i values were confirmed by Dixon plot after plotting the reciprocal of the rate of reaction against different concentrations of compounds **3b** and **3c** (Figs. 10C and 11C).

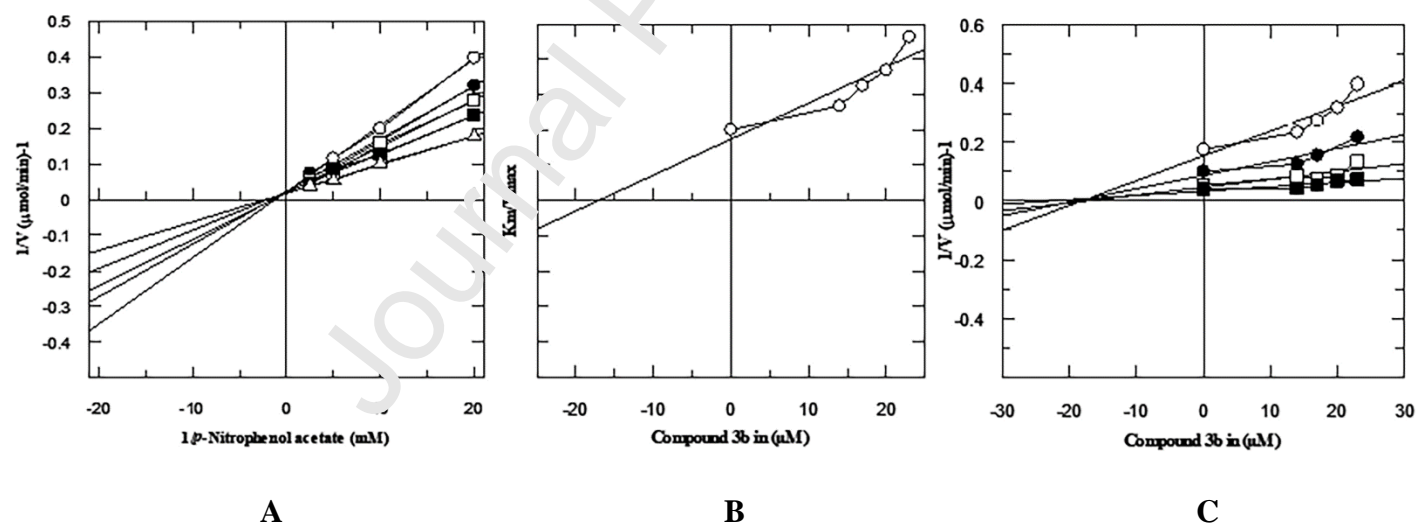


Fig. 10. The mode of inhibition of compound **3b** against *bCA-II*; (A) Lineweaver–Burk plot of the reciprocal rate of reaction (velocities) vs. reciprocal of substrate (*p*-nitrophenol acetate) in the absence (Δ), and presence of 14 μM (\blacksquare), 17 μM (\square), 20 μM (\bullet), and 23 μM (\circ) of compound **3b**. (B) Secondary re-plot of Lineweaver–Burk plot between the slopes of each line on Lineweaver–Burk plot vs. different concentrations of compound **3b**. (C) Dixon plot of the reciprocal rate of reaction (velocities) vs. different concentrations of compound **3b**.

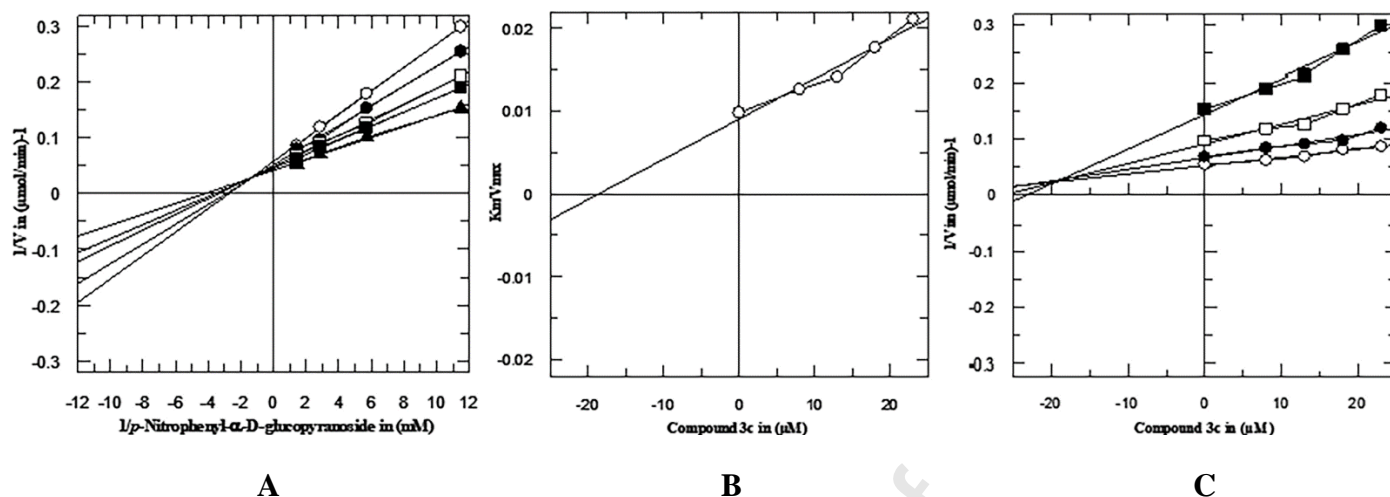


Fig. 11. The mode of inhibition of compound **3c** against α -glucosidase; (A) Lineweaver–Burk plot of the reciprocal rate of reaction (velocities) vs. reciprocal of substrate (*p*-nitrophenyl- α -D-glucopyranoside) in the absence (\blacktriangle), and presence of 8 μM (\blacktriangle), 13 μM (\square), 18 μM (\bullet), and 23 μM (\circ) of compound **3c**. (B) Secondary re-plot of Lineweaver–Burk plot between the slopes of each line on Lineweaver–Burk plot vs. different concentrations of compound **3c**. (C) Dixon plot of the reciprocal rate of reaction (velocities) vs. different concentrations of compound **3c**.

2.5. ADME properties

ADME properties predict the impact of therapeutic compounds to access the target considering some parameters. These properties can be evaluated using several prediction tools [49-51]. These properties help in the determination of the drug-likeness of compounds being used for drug discovery and development by sorting out new druggable candidates that are safer and follow the effective rules used for determination of these parameters. Below are some important ADME properties compiled using web service and its underlying methodologies (SwissADME) [49]. The results for all the designed compounds are reported in Table S2. The properties suggested that our derivatives are safer to use as drug candidates and have high probability of blood brain penetration and absorption.

2.5.1. Physicochemical properties

Some physicochemical and molecular descriptors are included in the properties such as molecular weight, number of specific atom types, molecular refractivity and polar surface area (calculated by fragmental technique called topological polar surface area (TPSA)), taking sulfur and phosphorus in account as polar atoms [52]. These descriptors are useful in prediction of ADME properties, with reference to biological barrier penetration like absorption and brain access [49].

2.5.2. Lipophilicity

The partition coefficient between water ($\log P_{o/w}$) and *n*-octanol demonstrates the classical descriptor of lipophilicity and some more freely available predictive models, like XLOGP3 (an atomistic method

including corrective factors and knowledge-based library), WLOGP (our own implementation of a purely atomistic method based on the fragmental system), MLOGP (an archetype of topological method relying on a linear relationship with 13 molecular descriptors), SILICOS-IT (an hybrid method relying on 27 fragments and 7 topological descriptors) and finally iLOGP (our in-house physics-based method relying on free energies of solvation in *n*-octanol and water calculated by the Generalized-Born and solvent accessible surface area (GB/SA) model).

2.5.3. Water solubility

Solubility is an important property enhancing absorption that greatly facilitates many drug development activities of molecules for discovery projects targeting oral administration. Two very well-established topological methods used for the prediction of water solubility in SwissADME [49], including an implementation of the ESOL model. These methods demonstrate strong linear correlation between predicted and experimental values ($R^2 = 0.69$ and 0.81 , respectively). Moreover, another predictor for solubility was developed by SILICOS-IT. All predicted values are the decimal logarithm of the molar solubility in water ($\log S$) providing the SwissADME solubility in mol/l and mg/ml.

2.5.4. Pharmacokinetics

The parameters in this section include the predictions for passive human gastrointestinal absorption (HIA) and blood-brain barrier (BBB) permeation, both are demonstrated in the BOILED-Egg model (Fig. 12) [51], in addition to the knowledge about compounds being substrate or non-substrate of the permeability glycoprotein (P-gp). The overexpression of P-gp is an important parameter to monitor in case of central nervous system and some tumor cells to investigate multidrug-resistance.

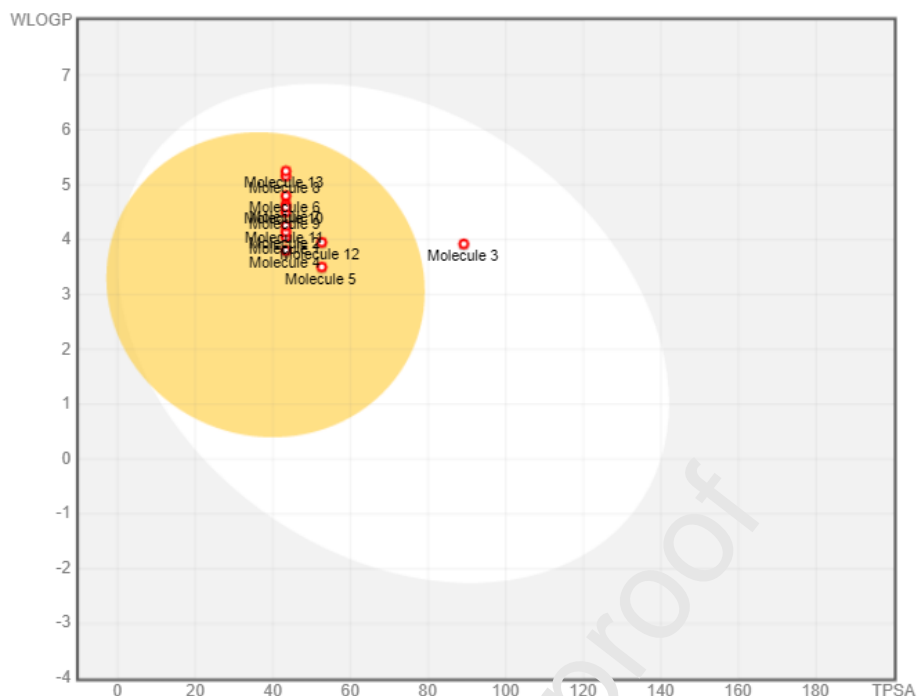


Fig. 12. The BOILED-Egg model predicts the position of molecules in the WLOGP versus TPSA [51].

The BOILED-Egg model predicts the intuitive evaluation of human intestinal absorption and brain penetration with reference to the position of molecules in the TPSA versus WLOGP. The model demonstrates the high probability of passive absorption by intestinal tract in white region, while yellow region demonstrates the high probability of blood brain penetration. Moreover, the red dots indicate that the molecules act as non-substrate of P-glycoprotein (PGP⁻). All the compounds were predicted as brain-penetrant (lies inside the yolk) and PGP⁻, except **3c** which is well absorbed but inaccessible to the brain (lies inside the white) and is not subject to active efflux (PGP⁻).

Another important parameter is the knowledge of molecules with reference to interactions with cytochromes P450 (CYP). This superfamily of isoenzymes is a key player in drug elimination through metabolic biotransformation. Literature showed that therapeutic molecules are substrate of five major isoforms (CYP1A2, CYP2C19, CYP2C9, CYP2D6, CYP3A4) and inhibition of these isoenzymes is certainly one major cause of pharmacokinetics-related drug-drug interactions. It is therefore of great importance for drug discovery to predict the tendency with which the molecule will cause significant drug interactions through inhibition of CYPs, and to determine which isoforms are affected.

2.5.5. Drug-likeness

Drug-likeness is a qualitative analysis of a molecule to become oral drug-candidate with enhanced bioavailability. The SwissADME properties include five different rule-based filters, with diverse

properties considering a molecule as drug-like. These filters often originate from analyses by major pharmaceutical companies aiming to improve the quality of their proprietary chemical collections.

2.5.6. Medicinal chemistry

The main purpose of these recognition methods is the identification of the potentially problematic fragments in a molecule. PAINS (for pan assay interference compounds) are molecules containing substructures showing potent response in assays irrespective of the protein target. Moreover, lead-likeness is a similar concept to drug-likeness and focuses on molecular entity acceptable for optimization and modification to enhance the size and lipophilicity, if required.

2.5.7. Toxicity

All the tested derivatives (**3a–m**) have been evaluated for their toxicology profile [53]. The compounds exhibited non-toxic liver profile and no cytotoxicity was noted (Table S2).

3. Conclusions

In summary, we have synthesized a series of keto ester derivatives **3a–m** through a facile coupling reaction of halogenated carboxylic acids and diversely substituted phenacyl bromides. The title keto esters were isolated in 72–82% yield. The *in vitro* inhibitory activities against α -glucosidase and carbonic anhydrase-II enzymes were evaluated and the results revealed that most of the compounds exhibit potent biological potential. Compound **3c** was identified as the lead inhibitor with an IC_{50} value of $12.4 \pm 0.16 \mu\text{M}$, 76-folds higher inhibitory efficacy compared to acarbose ($IC_{50} = 942 \pm 0.74 \mu\text{M}$). However, **3b** demonstrated the best result against carbonic anhydrase-II with an IC_{50} of $16.5 \pm 0.92 \mu\text{M}$ (acetazolamide; $IC_{50} = 18.2 \pm 1.23 \mu\text{M}$). The bioactivity results, influence of the substitution pattern and binding modes of the tested compounds were analyzed through molecular docking approach. The stabilization of the inhibitors in the active site of both enzymes was achieved through the formation of several conspicuous H-bonding interactions between the keto and ester functional groups and the amino acid residues. The evaluation of ADME properties such as physicochemical, pharmacokinetics, drug-likeness and medicinal chemistry affability by different methods such as iLOGP and BOILED-Egg, etc. suggests the safer pharmacological profile of all the screened derivatives.

4. Experimental

4.1. General chemistry methods

Unless otherwise noted, all materials were obtained from commercial suppliers (Aldrich and Merck companies) and used without further purification. Thin layer chromatography (TLC) was performed on Merck DF-Alufoilien 60F₂₅₄ 0.2 mm precoated plates. Product spots were visualized under UV light at 254. Melting points were recorded on a Stuart melting point apparatus (SMP3) and are uncorrected.

Infra-red (IR) spectra were recorded on FTS 3000 MX, Bio-Rad Merlin (Excalibur model) spectrophotometer. ^1H NMR spectra were recorded on a Bruker Avance (300 MHz) spectrometer. Chemical shifts (δ) are quoted in parts per million (ppm) downfield of tetramethylsilane, using residual solvent as internal standard (CDCl_3 at 7.24 ppm). Abbreviations used in the description of resonances are: s (singlet), d (doublet), t (triplet), q (quartet), m (multiplet), Ar (aromatic). Proton-decoupled ^{13}C NMR spectra were recorded on a Bruker Avance (75 MHz) spectrometer using deuterated solvent as internal standard (CDCl_3 at 77.23 ppm). Electron-spray ionization high resolution mass spectrometry (ESI-HRMS, m/z) data was acquired on an Agilent spectrometer (6530, Accurate Mass Q-TOF LC/MS).

4.2. General procedure for the preparation of keto ester derivatives (2a–m)

To a stirred solution of corresponding benzoic acids (**1a,b**) (1.0 mmol) in *N,N*-dimethylformamide (4 mL) was added triethylamine (3-4 drops) at room temperature. After stirring for 30 min, the corresponding phenacyl bromide (**2a–h**) (1.0 mmol) were added and the reaction mixture was stirred at room temperature for 2 h. After completion of reaction (monitored by TLC), the reaction mixture was washed with water and extracted with ethyl acetate (2×10 mL). The combined organic fractions were washed with brine (20 mL), dried over anhydrous MgSO_4 , filtered and evaporated *in vacuo*. The resultant solids were purified by recrystallization in ethanol to afford the corresponding keto esters (**3a–m**) [45-47]. The data was in full agreement to those reported in our previous work [47].

4.2.1. 2-(4-Fluorophenyl)-2-oxoethyl 2-bromobenzoate (3a)

Yield: 78%; m.p.: 98–99 °C; R_f : 0.55 (20% EtOAc/*n*-hexane); IR (ATR, cm^{-1}) 3015, 2950, 2840, 1732 ($\text{C}=\text{O}_{\text{ester}}$), 1697 ($\text{C}=\text{O}_{\text{keto}}$), 1594, 1506 ($\text{C}=\text{C}$); ^1H NMR (300 MHz, CDCl_3): δ_{H} 8.02–7.99 (m, 3H, ArH), 7.73–7.70 (m, 1H, ArH), 7.46–7.36 (m, 2H, ArH), 7.24–7.18 (m, 2H, ArH), 5.57 (s, 2H, OCH_2); ^{13}C NMR (75 MHz, CDCl_3): δ_{C} 192.9, 161.7 (d, $J = 255$ Hz), 163.0, 134.5, 133.1, 132.0, 131.0, 130.6, 130.5, 127.3, 122.1, 116.2 (d, $J = 21.7$ Hz), 66.5; HRMS (ESI+ve): exact mass calculated for $\text{C}_{15}\text{H}_{10}\text{BrFNaO}_3$ [$\text{M}+\text{Na}$] $^+$: 358.96950; found, 359.19800.

4.2.2. 2-(4-Chlorophenyl)-2-oxoethyl 2-bromobenzoate (3b)

Yield: 79%; m.p.: 94–96 °C; R_f : 0.25 (20% EtOAc/*n*-hexane); IR (ATR, cm^{-1}) 3085, 2932, 2868, 1724 ($\text{C}=\text{O}_{\text{ester}}$), 1698 ($\text{C}=\text{O}_{\text{keto}}$), 1584, 1471 ($\text{C}=\text{C}$); ^1H NMR (300 MHz, CDCl_3): δ_{H} 7.91–7.90 (m, 3H, ArH), 7.73–7.70 (m, 1H, ArH), 7.53–7.50 (m, 2H, ArH), 7.49–7.36 (m, 2H, ArH), 5.57 (s, 2H, OCH_2); ^{13}C NMR (75 MHz, CDCl_3): δ_{C} 192.9, 163.3, 140.6, 136.0, 134.5, 133.1, 132.4, 131.0, 129.3, 129.2, 127.3, 122.1, 66.5; HRMS (ESI+ve): exact mass calculated for $\text{C}_{15}\text{H}_{10}\text{BrClNaO}_3$ [$\text{M}+\text{Na}$] $^+$: 374.93995; found, 374.94533.

4.2.3. 2-(4-Nitrophenyl)-2-oxoethyl 2-bromobenzoate (3c)

Yield: 72%; m.p.: 92–94 °C; R_f : 0.14 (20% EtOAc/*n*-hexane); IR (ATR, cm^{-1}) 3045, 2946, 2837, 1725 ($\text{C}=\text{O}_{\text{ester}}$), 1698 ($\text{C}=\text{O}_{\text{keto}}$), 1574, 1491 ($\text{C}=\text{C}$); ^1H NMR (300 MHz, CDCl_3): δ_{H} 8.37–8.32 (m, 2H, ArH), 8.29–8.24 (m, 2H, ArH), 8.07–8.03 (m, 1H, ArH), 7.97–7.93 (m, 2H, ArH), 7.70–7.66 (m, 1H, ArH), 5.57 (s, 2H, OCH_2); ^{13}C NMR (75 MHz, CDCl_3): δ_{C} 190.1, 165.3, 148.8, 146.5, 138.7, 134.4, 133.3, 132.6, 132.1, 131.0, 129.9, 127.3, 66.4; HRMS (ESI+ve): exact mass calculated for $\text{C}_{15}\text{H}_{10}\text{BrNNaO}_5$ [$\text{M}+\text{Na}$] $^+$: 385.96400; found, 386.04910.

4.2.4. 2-Oxo-2-*p*-tolylethyl 2-bromobenzoate (3d)

Yield: 75%; m.p.: 91–93 °C; R_f : 0.27 (20% EtOAc/*n*-hexane); IR (ATR, cm^{-1}) 3031, 2924, 2844, 1728 ($\text{C}=\text{O}_{\text{ester}}$), 1685 ($\text{C}=\text{O}_{\text{keto}}$), 1603, 1481 ($\text{C}=\text{C}$); ^1H NMR (300 MHz, CDCl_3): δ_{H} 7.88 (d, 2H, $J = 8.4$ Hz, ArH), 7.72–7.69 (m, 2H, ArH), 7.45–7.37 (m, 2H, ArH), 7.36–7.28 (m, 2H, ArH), 5.57 (s, 2H, OCH_2), 2.45 (s, 3H, CH_3); ^{13}C NMR (75 MHz, CDCl_3): δ_{C} 192.6, 165.4, 145.1, 134.4, 133.0, 132.0, 131.6, 131.2 (2 \times C), 127.9, 127.3, 122.1, 66.5, 22.6; HRMS (ESI+ve): exact mass calculated for $\text{C}_{16}\text{H}_{13}\text{BrNaO}_3$ [$\text{M}+\text{Na}$] $^+$: 354.99458; found, 354.99304.

4.2.5. 2-(4-Methoxyphenyl)-2-oxoethyl 2-bromobenzoate (3e)

Yield: 80%; m.p.: 107–109 °C; R_f : 0.20 (20% EtOAc/*n*-hexane); IR (ATR, cm^{-1}) 3011, 2946, 2842, 1730 ($\text{C}=\text{O}_{\text{ester}}$), 1682 ($\text{C}=\text{O}_{\text{keto}}$), 1598, 1571 ($\text{C}=\text{C}$); ^1H NMR (300 MHz, CDCl_3): δ_{H} 7.98–7.96 (m, 1H, ArH), 7.95–7.94 (m, 2H, ArH), 7.72–7.69 (m, 1H, ArH), 7.46–7.35 (m, 2H, ArH), 7.02–6.97 (m, 2H, ArH), 5.58 (s, 2H, OCH_2), 3.90 (s, 3H, CH_3); ^{13}C NMR (75 MHz, CDCl_3): δ_{C} 191.3, 165.5, 143.8, 141.0, 134.4, 133.0, 132.0, 131.3, 130.2, 127.3, 122.1, 114.1, 66.5, 55.6; HRMS (ESI+ve): exact mass calculated for $\text{C}_{16}\text{H}_{13}\text{BrNaO}_4$ [$\text{M}+\text{Na}$] $^+$: 370.98949; found, 370.99396.

4.2.6 2-(3,4-Dichlorophenyl)-2-oxoethyl 2-bromobenzoate (3f)

Yield: 75%; m.p.: 84–86 °C; R_f : 0.23 (20% EtOAc/*n*-hexane); IR (ATR, cm^{-1}) 3101, 2926, 2844, 1728 ($\text{C}=\text{O}_{\text{ester}}$), 1701 ($\text{C}=\text{O}_{\text{keto}}$), 1584, 1489 ($\text{C}=\text{C}$); ^1H NMR (300 MHz, CDCl_3): δ_{H} 8.07 (d, 1H, $J = 2.1$ Hz, ArH), 8.04–8.01 (m, 1H, ArH), 7.80 (dd, 1H, $J = 8.4, 1.8$ Hz, ArH), 7.73–7.70 (m, 1H, ArH), 7.60 (s, 1H, ArH), 7.46–7.37 (m, 2H, ArH), 5.54 (s, 2H, OCH_2); ^{13}C NMR (75 MHz, CDCl_3): δ_{C} 189.9, 165.3, 134.8, 134.6, 133.8, 133.6, 133.5, 133.2, 132.3, 132.0, 131.1, 130.8, 129.9, 127.3, 66.5; HRMS (ESI+ve): exact mass calculated for $\text{C}_{15}\text{H}_9\text{BrCl}_2\text{NaO}_3$ [$\text{M}+\text{Na}$] $^+$: 408.90098; found, 408.93258.

4.2.7. 2-(Naphthalen-2-yl)-2-oxoethyl 2-bromobenzoate (3g)

Yield: 74%; m.p.: 88–90 °C; R_f : 0.34 (20% EtOAc/*n*-hexane); IR (ATR, cm^{-1}) 3054, 2925, 2847, 1732 ($\text{C}=\text{O}_{\text{ester}}$), 1687 ($\text{C}=\text{O}_{\text{keto}}$), 1625, 1590 ($\text{C}=\text{C}$); ^1H NMR (300 MHz, CDCl_3): δ_{H} 8.11–7.90 (m, 5H, ArH), 7.73–7.58 (m, 3H, ArH), 7.47–7.37 (m, 3H, ArH), 5.76 (s, 2H, OCH_2); ^{13}C NMR (75 MHz,

CDCl₃): δ_C 191.6, 165.5, 136.0, 134.5, 133.0, 132.4, 132.0, 131.5, 131.2, 129.7, 129.0, 127.9, 127.3, 127.1, 123.3, 122.1 (2 \times C), 118.4, 66.8; HRMS (ESI+ve): exact mass calculated for C₁₉H₁₃BrNaO₃ [M+Na]⁺: 390.99458; found, 391.09437.

4.2.8. 2-(Biphenyl-4-yl)-2-oxoethyl 2-bromobenzoate (3h)

Yield: 80%; m.p.: 101–103 °C; R_f: 0.48 (20% EtOAc/*n*-hexane); IR (ATR, cm⁻¹) 3037, 2933, 2842, 1732 (C=O_{ester}), 1692 (C=O_{keto}), 1600, 1560 (C=C); ¹H NMR (300 MHz, CDCl₃): δ_H 8.06–8.04 (m, 4H, ArH), 7.77–7.68 (m, 3H, ArH), 7.54–7.39 (m, 6H, ArH), 5.65 (s, 2H, OCH₂); ¹³C NMR (75 MHz, CDCl₃): δ_C 191.4, 165.4, 146.7, 139.6, 134.5, 133.1 (2 \times C), 132.8, 132.1, 131.2, 129.1, 128.5, 128.4, 127.6, 127.3, 122.1, 66.7; HRMS (ESI+ve): exact mass calculated for C₂₁H₁₅BrNaO₃ [M+Na]⁺: 417.01023; found, 417.01350.

4.2.9. 2-(4-Fluorophenyl)-2-oxoethyl 3-chloro-4-fluorobenzoate (3i)

Yield: 77%; m.p.: 121–123 °C; R_f: 0.61 (20% EtOAc/*n*-hexane); IR (ATR, cm⁻¹) 3054, 2955, 2834, 1723 (C=O_{ester}), 1702 (C=O_{keto}), 1592, 1496 (C=C); ¹H NMR (300 MHz, CDCl₃): δ_H 8.25 (dd, 1H, *J* = 8.7, 2.1 Hz, ArH), 8.08–7.99 (m, 3H, ArH), 7.29–7.19 (m, 3H, ArH), 5.57 (s, 2H, OCH₂); ¹³C NMR (75 MHz, CDCl₃): δ_C 190.1, 166.3 (d, *J* = 255 Hz), 164.1, 161.4 (d, *J* = 256 Hz), 132.8, 130.6, 130.5, 130.4, 126.5 (d, *J* = 3 Hz), 121.7 (d, *J* = 18 Hz), 116.8 (d, *J* = 21.8 Hz), 116.3 (d, *J* = 21.8 Hz), 66.5; HRMS (ESI+ve): exact mass calculated for C₁₅H₉ClF₂NaO₃ [M+Na]⁺: 333.01060; found, 333.17520.

4.2.10. 2-(4-Chlorophenyl)-2-oxoethyl 3-chloro-4-fluorobenzoate (3j)

Yield: 77%; m.p.: 121–123 °C; R_f: 0.61 (20% EtOAc/*n*-hexane); IR (ATR, cm⁻¹) 3052, 2939, 2845, 1717 (C=O_{ester}), 1698 (C=O_{keto}), 1538, 1494 (C=C); ¹H NMR (300 MHz, CDCl₃): δ_H 8.24 (dd, 1H, *J* = 7.2, 2.1 Hz, ArH), 7.93–7.90 (m, 2H, ArH), 7.28–7.22 (m, 4H, ArH), 5.56 (s, 2H, OCH₂); ¹³C NMR (75 MHz, CDCl₃): δ_C 190.6, 164.1, 161.4 (d, *J* = 255 Hz), 140.7, 132.6 (d, *J* = 39 Hz), 130.5, 130.4, 129.4, 129.2, 126.5 (d, *J* = 3.8 Hz), 121.7 (d, *J* = 18.8 Hz), 116.8 (d, *J* = 21.8 Hz), 66.6; HRMS (ESI+ve): exact mass calculated for C₁₅H₉Cl₂FNaO₃ [M+Na]⁺: 348.98105; found, 349.16330.

4.2.11. 2-Oxo-2-*p*-tolylethyl 3-chloro-4-fluorobenzoate (3k)

Yield: 82%; m.p.: 137–139 °C; R_f: 0.42 (20% EtOAc/*n*-hexane); IR (ATR, cm⁻¹) 3054, 2936, 2841, 1722 (C=O_{ester}), 1694 (C=O_{keto}), 1593, 1494 (C=C); ¹H NMR (300 MHz, CDCl₃): δ_H 8.83–8.22 (d, 2H, *J* = 7.5 Hz, ArH), 7.87 (d, 2H, *J* = 8.1 Hz, ArH), 7.34–7.22 (m, 3H, ArH), 5.59 (s, 2H, OCH₂), 2.46 (s, 3H, CH₃); ¹³C NMR (75 MHz, CDCl₃): δ_C 191.2, 164.2, 161.3 (d, *J* = 255 Hz), 145.1, 132.8, 131.5, 130.5, 130.4, 129.7, 127.9, 126.7 (d, *J* = 3.8 Hz), 116.8 (d, *J* = 21.8 Hz), 66.7, 22.6; HRMS (ESI+ve): exact mass calculated for C₁₆H₁₂ClFNaO₃ [M+Na]⁺: 329.03567; found, 329.19800.

4.2.12. 2-(4-Methoxyphenyl)-2-oxoethyl 3-chloro-4-fluorobenzoate (3l)

Yield: 78%; m.p.: 134–136 °C; R_f: 0.35 (20% EtOAc/*n*-hexane); IR (ATR, cm⁻¹) 3048, 2941, 2844, 1720 (C=O_{ester}), 1687 (C=O_{keto}), 1594, 1573 (C=C); ¹H NMR (300 MHz, CDCl₃): δ_H 8.26 (dd, 1H, *J* = 6.9, 2.1 Hz, ArH), 8.09–8.04 (m, 1H, ArH), 7.98–7.93 (m, 2H, ArH), 7.26 (d, 1H, *J* = 8.7 Hz, ArH), 7.02–6.97 (m, 2H, ArH), 5.56 (s, 2H, OCH₂), 3.91 (s, 3H, OCH₃); ¹³C NMR (75 MHz, CDCl₃): δ_C 190.0, 164.2, 161.3 (d, *J* = 255 Hz), 132.8, 130.3 (d, *J* = 8 Hz), 130.1, 127.1, 126.8, 126.7, 121.6 (d, *J* = 18 Hz), 116.8 (d, *J* = 21 Hz), 114.2, 66.5, 55.6; HRMS (ESI+ve): exact mass calculated for C₁₆H₁₂ClFNaO₄ [M+Na]⁺: 345.03058; found, 345.04408.

4.2.13. 2-(3,4-Dichlorophenyl)-2-oxoethyl 3-chloro-4-fluorobenzoate (3m)

Yield: 75%; m.p.: 110–112 °C; R_f: 0.53 (20% EtOAc/*n*-hexane); IR (ATR, cm⁻¹) 3064, 2973, 2938, 1718 (C=O), 1699 (C=O_{keto}), 1582, 1494 (C=C); ¹H NMR (300 MHz, CDCl₃): δ_H 8.24–8.17 (m, 1H, ArH), 8.08–8.02 (m, 2H, ArH), 7.80 (dd, 1H, *J* = 8.4, 2.1 Hz, ArH), 7.63 (d, 1H, *J* = 8.4 Hz, ArH), 7.29–7.23 (m, 1H, ArH), 5.54 (s, 2H, OCH₂); ¹³C NMR (75 MHz, CDCl₃): δ_C 189.8, 164.0, 161.7 (d, *J* = 255 Hz), 138.9, 133.9, 133.5, 133.1, 132.9, 131.2, 130.5 (d, *J* = 8.3 Hz), 129.9, 126.5 (d, *J* = 37.5 Hz), 121.8 (d, *J* = 18.7 Hz), 116.9 (d, *J* = 21.8 Hz), 66.5; HRMS (ESI+ve): exact mass calculated for C₁₅H₈Cl₃FNaO₃ [M+Na]⁺: 382.94208; found, 382.92115.

4.3. Bioassay protocols

4.3.1. *In vitro* α-glucosidase inhibition assay

In vitro α-glucosidase inhibitory activity was determined according to the previously developed fluorimetric protocol [54]. The total assay solution comprised of enzyme (0.2 unit/well) prepared in phosphate buffered saline (PBS) (100 mM, pH 6.8) with different concentrations of samples (1–0.0312 mM) at 37 °C were incubated for 15 min. All test compounds were solubilized in HPLC grade DMSO (7.5% final volume) along with negative and positive controls. After pre-incubation, the reaction was started by adding 20 μL of substrate *p*-nitrophenyl-α-D-glucopyranoside (0.7 mM) and continuous changes in absorbance was measured at 400 nm for 30 min by microplate spectrophotometer (xMark™, BIO-RAD, California, LA, United States). Acarbose (specific inhibitor) with IC₅₀ value of 942.2 ± 0.74 μM was used as a reference drug. The IC₅₀ values were calculated by using different concentrations of tested compounds. The results were processed and analyzed by MS-Excel and Ez-fit software programs. The % inhibition of each compound was calculated using the following formula:

$$\% \text{ Inhibition} = 100 - \left(\frac{\text{OD test well}}{\text{OD control}} \right) \times 100$$

4.3.2. *In vitro* carbonic anhydrase-II inhibition assay

In-vitro bCA-II activity was measured by following the spectrophotometric method described by Pocker and Meany with slight modifications [55,56]. The spectrophotometric assay was conducted in HEPES-Tris buffer of pH 7.4 (20 mM) at 25 °C. Each inhibitory well consists of 140 μ L of HEPES-Tris buffer solution, 20 μ L of bCA-II enzyme solution (0.1 mg/mL HEPES-Tris buffer) and 20 μ L of test compound in HPLC grade DMSO (maintain 10% of the final concentration). The mixture solution was pre-incubated for 15 min at 25 °C. Substrate *p*-nitrophenol acetate (0.7 mM) was prepared in HPLC grade methanol and the reaction was started by adding 20 μ L to well in 96-well plate. The continuous measurement of amount of product formed at 400 nm for 30 min at 1 min interval in 96-well plate, using xMARK microplate spectrophotometer, Bio-Rad (USA). The activity of controlled compound was taken as 100%. All experiments were carried out in triplicate of each used concentration, and results are represented as mean of the triplicate. The % inhibition of each compound was calculated using the following formula:

$$\% \text{ Inhibition} = 100 - \left(\frac{\text{O.D. test well}}{\text{O.D. control}} \right) \times 100$$

4.3.3. Statistical Analysis

The EZ-Fit Enzyme Kinetics program (Genella Scientific Inc., Amherst, USA) was employed to calculate the IC₅₀ values. All graphs were plotted using GraFit program (1999). Values of the correlation coefficients, intercepts, slopes, and their standard errors were calculated by the linear regression analysis using the same program. Each point in the constructed graphs represents the mean of the three experiments [57].

4.4. Molecular docking protocol

The molecular modeling studies were carried out using Molecular Operating Environment (MOE, 2014.14). The structures of the compounds were prepared by ChemDraw and minimized on MOE until an RMSD gradient of 0.1 kcal·mol⁻¹Å⁻¹ was achieved with MMFF94x force field. During minimization, partial charges were automatically calculated, and the structures were transformed into three-dimensional form. The X-ray crystallographic structure of CA-II (PDB ID: 1V9E, resolution: 1.95Å) was downloaded from the RCSB Protein Data Bank (<https://www.rcsb.org>), while the 3D-structure of *Saccharomyces cerevisiae* α -glucosidase was prepared by homology modeling. The detailed procedure is discussed in our previous reports [56,58]. The enzyme structures were then prepared for the molecular docking simulation using Protonate 3D protocol in MOE with its default

parameters. The docking was performed using Triangle Matcher placement method and London dG scoring function.

Declaration of competing interest

The authors declare that they have no known competing financial interests or personal relationships that could have appeared to influence the work reported in this paper.

References

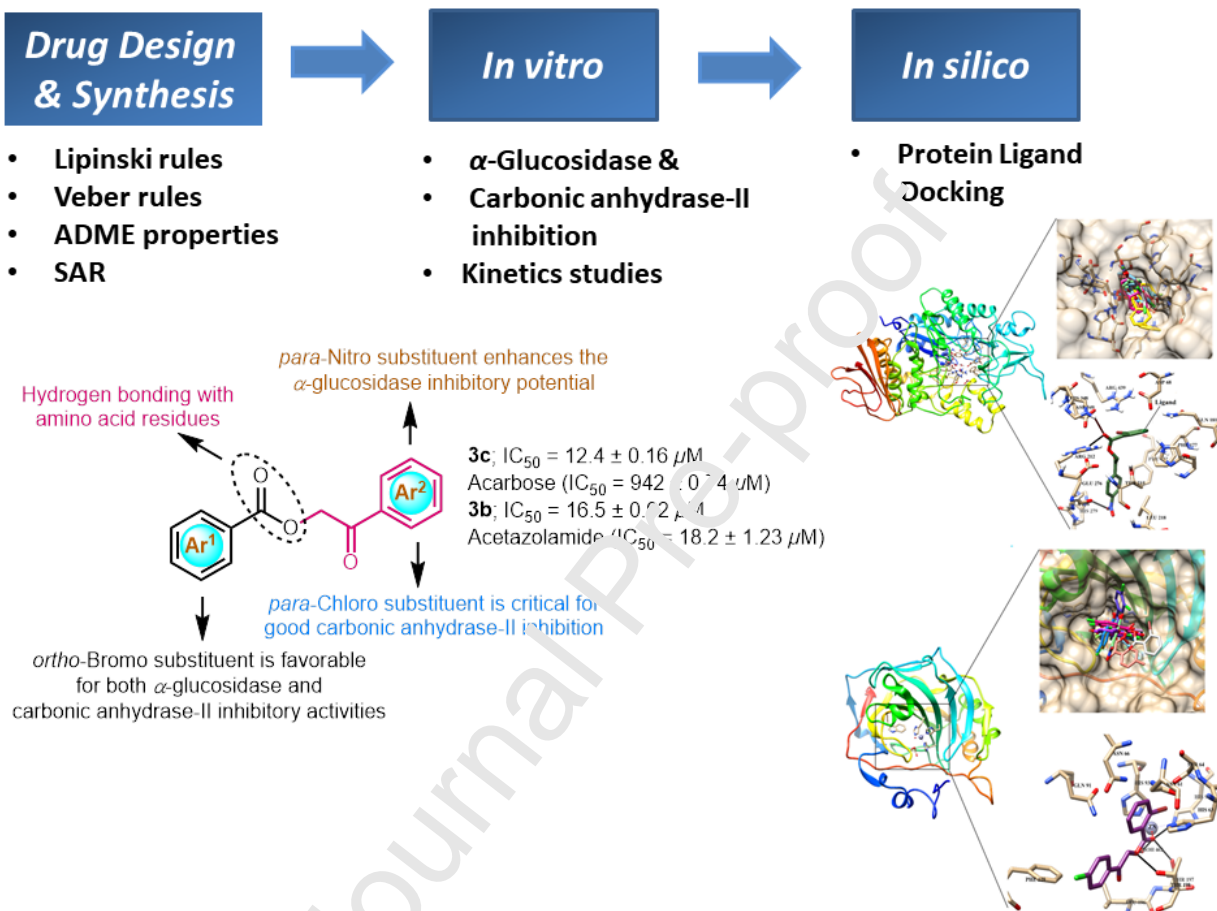
- [1] N. Kerru, A. Singh-Pillay, P. Awolade, P. Singh, *Eur. J. Med. Chem.* 152 (2018) 436-488.
- [2] P. Raigond, B. Kaundal, A. Sood, S. Devi, S. Dutt, R. Li, B. Singh, *J. Food Compos. Anal.* 74 (2018) 82-88.
- [3] S.H. Ley, A.V.A. Korat, Q. Sun, D.K. Tobias, C. Zhang, L. Qi, W.C. Willett, J.E. Manson, F.B. Hu, *Am. J. Public Health* 106 (2016) 1624-1630.
- [4] A. Migdal, M. Abrahamson, A. Peters, N. Vint, *Ann. Med.* (2015) 1-27.
- [5] T. Wilke, B. Boettger, B. Berg, A. Groth, S. Mueller, M. Potteman, S. Yu, A. Fuchs, U. Maywald, *J. Diabetes Complicat.* 29 (2015) 1015-1023.
- [6] A.D. Deshpande, M. Harris-Hayes, M. Schootman, *Phys. Ther.* 88 (2008) 1254-1264.
- [7] A.B. Olokoba, O.A. Obateru, L.B. Olokoba, *Clin. Med. J.* 27 (2012) 269-73.
- [8] L.M. Muller, K.J. Gorter, E. Hak, W.L. Goudzwaard, F.G. Schellevis, A.I. Hoepelman, G.E. Rutten, *Clin. Infect. Dis.* 41 (2005) 281-288.
- [9] S.K. Garg, H. Maurer K. Reed, R. Seta Ramsetty, *Diabetes Obes. Metab.* 16 (2014) 97-110.
- [10] J.C. Pickup, *Nat. Rev. Endocrinol.* 13 (2017) 568-577.
- [11] U. Ghani, *Eur. J. Med. Chem.* 103 (2015) 133-162.
- [12] A. Trapero, A. Llebaria, *J. Med. Chem.* 55 (2012) 10345-10346.
- [13] M. Saeedi, M. Mohammadi-Khanaposhtani, P. Pourrabia, N. Razzaghi, R. Ghadimi, S. Imanparast, M.A. Faramarzi, F. Bandarian, E.N. Esfahani, M. Safavi, H. Rastegar, B. Larijani, M. Mahdavi, T. Akbarzadeh, *Bioorg. Chem.* 83 (2019) 161-169.
- [14] F. Hussain, Z. Khan, M.S. Jan, S. Ahmad, A. Ahmad, U. Rashid, F. Ullah, M. Ayaz, A. Sadiq, *Bioorg. Chem.* 91 (2019) 103128.
- [15] M. Adib, F. Peytam, M. Rahmanian-Jazi, S. Mahernia, H.R. Bijanzadeh, M. Jahani, M. Mohammadi-Khanaposhtani, S. Imanparast, M.A. Faramarzi, M. Mahdavi, B. Larijani, *Eur. J. Med. Chem.* 155 (2018) 353-363.
- [16] C.M.M. Santos, M. Freitas, E. Fernandes, *Eur. J. Med. Chem.* 157 (2018) 1460-1479.
- [17] M. Dhameja, P. Gupta, *Eur. J. Med. Chem.* 176 (2019) 343-377.

- [18] H. Sun, Y. Zhang, W. Ding, X. Zhao, X. Song, D. Wang, Y. Li, K. Han, Y. Yang, Y. Ma, R. Wang, D. Wang, P. Yu, *Eur. J. Med. Chem.* 123 (2016) 365-378.
- [19] G. Wang, Z. Peng, J. Wang, X. Li, J. Li, *Eur. J. Med. Chem.* 125 (2017) 423-429.
- [20] F. Ali, K.M. Khan, U. Salar, M. Taha, N.H. Ismail, A. Wadood, M. Riaz, S. Perveen, *Eur. J. Med. Chem.* 138 (2017) 255-272.
- [21] G.-J. Ye, T. Lan, Z.-X. Huang, X.-N. Cheng, C.-Y. Cai, S.-M. Ding, M.-L. Xie, B. Wang, *Eur. J. Med. Chem.* 177 (2019) 362-373.
- [22] X.-T. Xu, X.-Y. Deng, J. Chen, Q.-M. Liang, K. Zhang, D.-L. Li, P.-P. Wu, X. Zheng, R.-P. Zhou, Z.-Y. Jiang, A.-J. Ma, W.-H. Chen, S.-H. Wang, *Eur. J. Med. Chem.* 189 (2020) 112013.
- [23] Z. Weiwei, R. Hu, *Biochem. Biophys. Res. Commun.* 390 (2009) 368-371.
- [24] G. Adamus, S. Yang, R.G. Weleber, *Exp. Eye Res.* 147 (2016) 161-168.
- [25] R. Williams, M. Airey, H. Baxter, J. Forrester, T. Kennedy-Martin, A. Girach, *Eye* 18 (2004) 963-983.
- [26] R. Klein, B.E. Klein, S.E. Moss, K.J. Cruickshanks, *Ophthalmology* 105 (1998) 1801-1815.
- [27] B. Becker, *Am. J. Ophthalmol.* 37 (1954) 13-15.
- [28] C.T. Supuran, *Nat. Rev Drug Discov.* 7 (2008) 168-181.
- [29] C.T. Supuran, *J. Enzyme Inhib. Med. Chem.* 31 (2016) 345-360.
- [30] F. Mincione, A. Scozzafava, C.T. Supuran, *Curr. Pharm. Des.* 14 (2008) 649-654.
- [31] I.P. Kaur, R. Smitha, D. Aggarwal, M. Kapil, *Int. J. Pharm.* 248 (2002) 1-14.
- [32] A. Ibrar, S. Zaib, I. Khan, Z. Shafique, A. Saeed, J. Iqbal, *J. Taiwan Inst. Chem. Eng.* 81 (2017) 119-133.
- [33] M. Kazmi, S. Zaib, A. Ibrar, S.T. Amjad, Z. Shafique, S. Mehsud, A. Saeed, J. Iqbal, I. Khan, *Bioorg. Chem.* 77 (2018) 197-202.
- [34] B. Stanovnik, J. Svete, *Chem. Rev.* 104 (2004) 2433-2480.
- [35] H. Sheibani, M.R. Islami, A. Hassanpur, K. Saidi, *Phosphorus Sulfur Silicon Relat. Elem.* 183 (2007) 13-20.
- [36] H. Sheibani, M.H. Mosslemin, S. Behzadi, M.R. Islami, K. Saidi, *Synthesis* 3 (2006) 435-439.
- [37] S. Pal, J. Mareddy, N.S. Devi, *J. Braz. Chem. Soc.* 19 (2008) 1207-1214.
- [38] S. Cen, X. Lv, Y. Jiang, A. Fakhri, V.K. Gupta, *Catal. Sci. Technol.* 10 (2020) 6687-6693.
- [39] M. Yang, F. Lu, T. Zhou, J. Zhao, C. Ding, A. Fakhri, V.K. Gupta, *J. Photochem. Photobiol. B*, 212 (2020) 112025.

- [40] J. Zhang, E. Ding, S. Xu, Z. Li, A. Fakhri, V.K. Gupta, *Int. J. Biol. Macromol.* 164 (2020) 1584–1591.
- [41] M. Huang, R. Zhang, Z. Yang, J. Chen, J. Deng, A. Fakhri, V.K. Gupta, *Int. J. Biol. Macromol.* 162 (2020) 220–228.
- [42] H. Wang, G. Li, A. Fakhri, *J. Photochem. Photobiol. B*, 207 (2020) 111882.
- [43] G. Wang, A. Fakhri, *Int. J. Biol. Macromol.* 155 (2020) 36–41.
- [44] M. Lu, Y. Cui, S. Zhao, A. Fakhri, *J. Photochem. Photobiol. B*, 205 (2020) 111842.
- [45] I. Khan, A. Ibrar, A. Korzański, M. Kubicki, *Acta Cryst. E*68 (2012) o3465.
- [46] I. Khan, A. Ibrar, S. Hameed, J.M. White, J. Simpson, *Acta Cryst. E*70 (2014) 301–304.
- [47] I. Khan, A. Saeed, M.I. Arshad, J.M. White, *Pak. J. Pharm. Sci.* 29 (2016) 39–49.
- [48] F. Tümer, D. Ekinci, K. Zilbeyaz, Ü. Demir, *Turk. J. Chem.* 28 (2004) 395–403.
- [49] A. Daina, O. Michielin, V. Zoete, *Sci. Rep.* 7 (2017) 42717.
- [50] A. Daina, O. Michielin, V. Zoete, *J. Chem. Inf. Model.* 54 (2014) 3284–3301.
- [51] A. Daina, V. Zoete, *ChemMedChem* 11 (2016) 1117–1121.
- [52] P. Ertl, B. Rohde, B. P. Selzer, *J. Med. Chem.* 43 (2000) 3714–3717.
- [53] <https://vnnadmet.bhsai.org/vnnadmet/login.aspx>
- [54] N.U. Rehman, A. Khan, A. Al-Harrasi, H. Hussain, A. Wadood, M. Riaz, Z. Al-Abri, *Bioorg. Chem.* 79 (2018) 27–33.
- [55] Y. Pocker, J. Meany, *Biochemistry* 6 (1967) 239–246.
- [56] N.U. Rehman, S.A. Halim, M. Al-Azri, M. Khan, A. Khan, K. Rafiq, A. Al-Rawahi, R. Csuk, A. Al-Harrasi, *Biomolecules*, 10 (2020) 751.
- [57] R.J. Leatherbarrow, *Green* Version 4.09. 1999, E.S.L. Staines, UK.
- [58] N.U. Rehman, K. Rafiq, A. Khan, S.A. Halim, L. Ali, N. Al-Saady, A.H. Al-Balushi, A. Al-Harrasi, *Mar. Drugs*, 17 (2019) 666.

Graphical abstract

The present study investigates the dual inhibitory potential of a series of keto ester derivatives against α -glucosidase and carbonic anhydrase-II enzymes.



CRedit authorship contribution statement

Imtiaz Khan: Conceptualization, Supervision, Synthesis, Writing – review & editing original draft, Formal analysis, Investigation, Visualization, **Ajmal Khan:** Biological activities, **Sobia Ahsan Halim:** Computational analysis, **Majid Khan:** Biological activities, **Sumera Zaib:** ADME properties, **Balqees Essa Mohammad Al-Yahyaei:** Biological activities, **Ahmed Al-Harrasi:** Supervision, Resources, **Aliya Ibrar:** Synthesis & characterization, Writing, Data investigation.

Highlights

- New structural libraries of compounds were prepared to treat diabetes mellitus and diabetic retinopathy
- Keto esters **3a-m** were investigated as potent inhibitors of α -glucosidase and carbonic anhydrase-II enzymes
- Compound **3c** was identified as the most potent inhibitor of α -glucosidase enzyme
- Compound **3b** inhibited the carbonic anhydrase-II with an IC_{50} of $16.5 \pm 0.92 \mu M$
- Molecular docking, enzyme kinetics, and detailed ADMET properties were also investigated